A Non-rare-Earth Ions Self-Activated White Emitting Phosphor under Single Excitation

Hongyu Guo, Junying Zhang, Lun Ma, Jose L. Chavez, Luqiao Yin, Hong Gao, Zilong Tang, and Wei Chen**

White light phosphors have many potential applications such as solid-state lighting, full color displays, light source for plant growth, and crop improvement. However, most of these phosphors are rare-earth-based materials which are costly and would be facing the challenge of resource issue due to the extremely low abundance of these elements on earth. A new white color composite consisted of a graphitic-phase nitrogen carbon (g-C_3N_4) treated with nitric acid and copper-cysteamine $Cu_3Cl(SR)_2$ is reported herein. Under a single wavelength excitation at 365 nm, these two materials show a strong blue and red luminescence, respectively. It is interesting to find that the white light emission with a quantum yield of 20% can be obtained by mixing these two self-activated luminescent materials at the weight ratio of 1:1.67. Using a 365 nm near-ultraviolet chip for excitation, the composite produces a white light-emitting diode that exhibits an excellent color rendering index of 94.3. These white-emitting materials are environment friendly, easy to synthesize, and cost-effective. More importantly, this will potentially eliminate the challenge of rare earth resources. Furthermore, a single chip is used for excitation instead of a multichip, which can greatly reduce the cost of the devices.

1. Introduction

Lighting and displays are the basic needs for our daily life—from television, mobile phone, illumination light, emergency light for safety, as well as to radiation and biological detection, drug delivery, and bioimaging for our security.[1,2] In addition, luminescence materials may convert the ultraviolet (UV) of the sunshine to blue and red light for photosynthesis enhancement so as to increase crop yields.[3–7] Crop yield is mainly dependent on photosynthesis which is a process used by plants and other organisms to convert light energy, normally from the Sun, into chemical energy that can be later released to fuel the organisms' activities. The plant photosynthesis strongly depends on the total amount of light received by the plant in the photosynthetic active radiation ranging from 400 to 700 nm with major contributions from the blue (400–500 nm) and red light (600–700 nm).[8,9] To improve the sunlight conversion efficiency of the photosynthetic process is to convert unused portions of sunlight to blue and red light.

Numerous efforts have been dedicated to the research and development of luminescence materials for these applications and most phosphors are rare-earth-based materials. For example, the three basic phosphors for solid state lighting are materials doped with Eu^{3+} (red), Tb^{3+} (green), and Eu^{2+} (blue).[10–15] The most tested luminescence or light converting materials for photosynthesis improvement are Eu^{2+}-doped sulfates[4,6] and silicate phosphors.[7] The advantage is that these materials have a high light output that can meet the requirement for these applications. However, the challenging issue is that rare earths are very expensive and their resources are very limited due to the extremely low abundance of these elements on earth. One alternative solution is to explore non-rare-earth materials that can fulfill these requirements for practical applications, which represents a new research direction for luminescence, or/and light converting materials. For example, defect-related luminescence materials without rare earth are stable, efficient, and less toxic, being free of the burdens of intrinsic toxicity or elemental scarcity, and the need for stringent, intricate, tedious, costly, or inefficient preparation steps.[2] Here, for the first time, we report white color non-rare-earth composites consisted of a graphitic-phase nitrogen carbon (g-C_3N_4) and copper-cysteamine $Cu_3Cl(SR)_2$. Our preliminary results show that these composites can produce strong white light which can be used for solid-state lighting, full color displays and as light source for plant growth, and crop improvement.

Recently, carbon nitrides have become a hot topic in scientific community due to their unique properties such as high

H. Guo, Prof. J. Zhang, Dr. H. Gao
Department of Physics
Beihang University
Beijing 100191, China
E-mail: zjy@buaa.edu.cn
Dr. L. Ma, J. L. Chavez, Prof. W. Chen
Department of Physics
University of Texas at Arlington
Arlington, TX 76019, USA
E-mail: weichen@uta.edu
Prof. L. Yin
Key Laboratory of Advanced Display and
System Applications (Shanghai University)
Ministry of Education
Shanghai 200072, China
Prof. Z. Tang
State Key Laboratory of New Ceramics and Fine Processing
School of Materials Science and Engineering
Tsinghua University
Beijing 100084, China

DOI: 10.1002/adfm.201502641

photocatalytic activity, luminescence, chemical stability as well as free of metal elements.[16–18] They have several allotropes with various properties, and g-C_3N_4 is regarded as the most stable allotrope under ambient environment.[17,18] g-C_3N_4 is abundant and can be easily obtained via one-step polymerization of cheap precursor such as cyanamide,[17,20] urea,[19,21,22] thiourea,[23] melamine,[24,25] and dicyandiamide.[26] The band gap of g-C_3N_4 is 2.7 eV as estimated from absorption spectrum and it decreases as the condensation temperature increases. As a good photocatalyst, the g-C_3N_4 can split water to generate hydrogen or/and oxygen under visible light irradiation. As a good phosphor with strong luminescence, g-C_3N_4 can be used for solid state lighting, displays, and sensing. The nanoscale g-C_3N_4 such as nanopowder, nanosheet, and nanoparticles in mesoporus silica and single-layer nanodots have intense luminescence, while the luminescence of bulk g-C_3N_4 is quite weak (4.8%).[16,27–29] Many efforts have been dedicated to improve the luminescence quantum yield of bulk g-C_3N_4. The ultrathin g-C_3N_4 nanosheets obtained by a "green" liquid exfoliation route exhibit a quantum yield of 19.6%.[28] The graphitic carbon nitride quantum dots (g-CNQDs) synthesized with a low-temperature solid-phase method show a quantum yield of 42%.[30] Here we report a new and simple method that can more than triple the luminescence intensity of g-C_3N_4. We also explore the white color emission from the composites made with g-C_3N_4 and copper-cysteamine (Cu-Cy)—a new material that can produce singlet oxygen and red light when excited by X-ray or UV light.[31,32] Our goal is to demonstrate that white light can be obtained through a good combination of these two materials and the white emission can be realized with only one chip for excitation.

2. Results and Discussion

Figure 1 shows the emission and excitation spectra for the as-prepared g-C_3N_4, the treated g-C_3N_4 by nitric acid, and Cu-Cy at room temperature. The as-prepared g-C_3N_4 shows a bright blue luminescence at 461 nm when excited at 365 nm. The emission peaks of the acid treated g-C_3N_4 samples are at 441, 438, and 435 nm, respectively. The emission of the treated samples is shifted to shorter wavelengths as compared with that of the as-prepared sample, and the blueshift is larger if the acid concentration is higher. For the sample treated with 60.7% of nitric acid, the blue-shift is up to 26 nm. More interesting, the luminescence intensity is greatly enhanced. The quantum yield of the as-prepared g-C_3N_4 is only 5.9%, while for the sample treated with 60.7% nitric acid, the quantum yield is improved up to 11.8%. For the sample treated with the 60.7% nitric acid, the intensity has more than tripled. The blueshift is likely due to the quantum size effect as the acidification may convert the bulk g-C_3N_4 into nanoparticles. Consequently, the conduction and valence bands shift in opposite directions and the energy gap opens up.[28]

The XRD patterns of the carbon nitride obtained at 500 °C and the g-C_3N_4 treated with nitric acid are shown in **Figure 2**. The XRD pattern of the g-C_3N_4 synthesized at 500 °C exhibits two typical peaks. The intense peak at 27.4° is associated with an interlayer distance d = 0.326 nm and is indexed for graphitic carbon nitride as the (002) plane. It represents the characteristic interplanar stacking of aromatic systems.[33] The weak diffraction peak at 13.1° corresponds to the in-plane structural packing motif indexed as the (100) plane.[30]

After the acid treatment, the peak at 13° gradually decreases and finally disappears, and the peak at 27.4° shifts to 27.9°. This means that the acid treatment did affect the crystal structure of g-C_3N_4. The bulk g-C_3N_4 are composed of small particles about 200 nm as shown by the SEM images in **Figure 3**a,b as well as the TEM image in Figure 3e. After treating with nitric acid, some g-C_3N_4 were delaminated as shown by the SEM image in Figure 3c. The layer-like powders are composed with much smaller particles, and some are as small as 15 nm as seen in Figure 3d,f. The decrease in the particle size accounts for the gradual weakening and the disappearance of the low-angle reflection peak at 13° as a consequence of the destruction in the long-range order of the in-plane structural packing.[16,34,35] The delamination of the bulk materials causes the shift of the peak at 27° because of the shrinking of the distance between the sheets. The single layers in bulk g-C_3N_4 are potentially undulated, but could be planarized by heating using nitric acid, resulting in a denser stacking.[16,35] The photoluminescence of g-C_3N_4 was ascribed to the electron transition between valence and conduction band. Under UV light irradiation, electron is

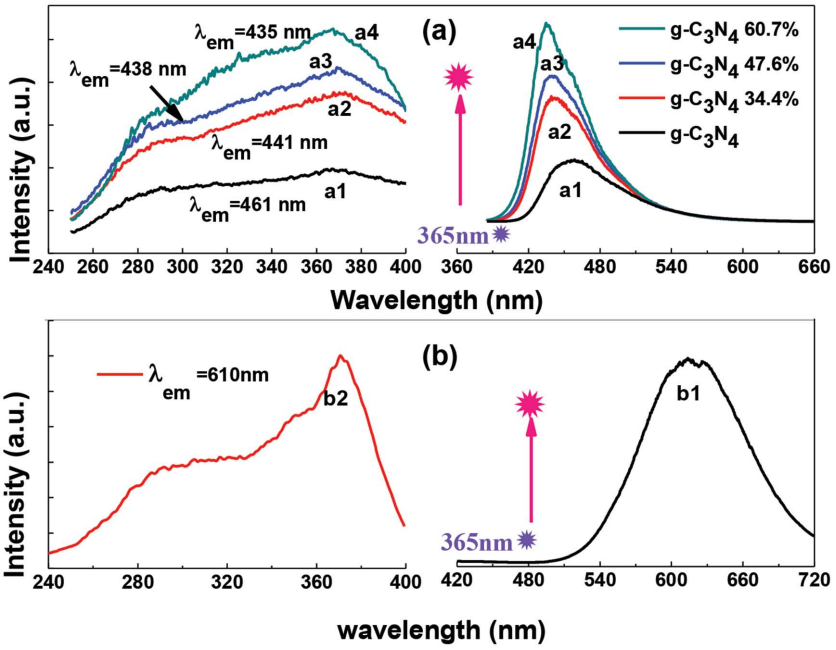

Figure 1. Photoluminescence a) excitation and emission spectra of the pristine g-C_3N_4 synthesized at 500 °C (a1) and the samples treated by nitric acid with different concentrations (a2: 34.4%; a3: 47.6%; a4: 60.7%) at 365 nm excitation, b) emission spectra of Cu-Cy excited at 365 nm (b1) and the excitation spectra by monitoring emission at 610 nm (b2).

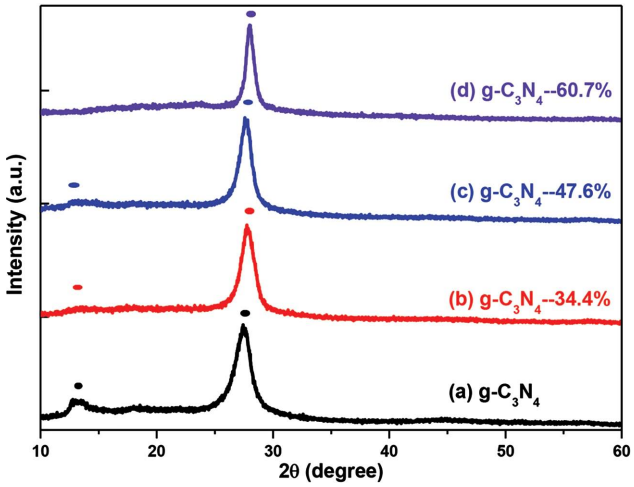

Figure 2. The XRD patterns of a) the g-C_3N_4 synthesized at 500 °C and b–d) the treated samples by nitric acid with different concentrations.

excited from the δ valence band to δ^* conduction band. The electron relaxing to the π^* conduction band returns to the lone pair (LP) valance band, leading blue emission.[27] The calculated density of states (DOS) of single-layered g-C_3N_4 nanosheets shows an obvious increase of DOS at the conduction band edge with respect to the bulk counterpart, indicating the g-C_3N_4 nanosheets possess more charge carriers.[28] Thus, one can anticipate that the delaminated g-C_3N_4 may have improved photosensitivity. The delamination along with the formation of nanoscale size particles cause the blueshift of the absorption edge (Figure S1, Supporting Information) and emission peak as

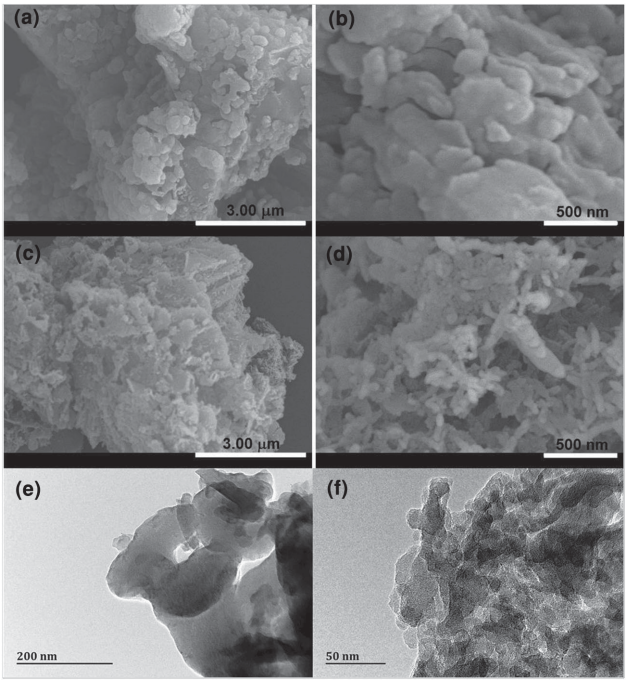

Figure 3. The SEM images of a,b) the g-C_3N_4 obtained at 500 °C and c,d) the treated sample using 60.7% nitric acid and TEM images of e) g-C_3N_4 obtained at 500 °C and f) the treated sample using 60.7% nitric acid.

a result of quantum size effect. As the nitric acid concentration is increased, more and more delaminations occur, and more and more nanoparticles are formed, thus the emission shows a continuous blue-shift and the emission intensity is gradually enhanced.

Cu-Cy is a new material with a new structure in which both the thio and amine groups form cysteamine bonding with the copper ions. The Cu-Cy particles include two different Cu atoms—Cu(1) and Cu(2). The valence analyses from single crystal X-ray diffraction and solid-state nuclear magnetic spectroscopy have shown that they are both Cu^+ ions.[31] The emission of the Cu-Cy is broadband emission with main peak at 613 nm and a slightly-lower peak at 626 nm when excited at 365 nm as shown in Figure 1b. It is interesting that g-C_3N_4 and Cu-Cy have similar excitation spectra, i.e., both have broad excitation band ranging from 250 to 420 nm with a maximum at about 365 nm. This indicates that the two luminescent materials can be activated using a single wavelength excitation. The absorption spectrum of Cu-Cy has a sharp absorption edge at 399 nm which is corresponding to a band gap of 3.11 eV (see **Figure 4**). g-C_3N_4 show almost no emission below 400 nm as shown in Figure 1a, i.e., the blue emission of g-C_3N_4 is not obviously overlapped with the absorption of Cu-Cy, therefore, no reabsorption or energy transfer occurs between the two materials.

The band structure and DOS of Cy-Cu calculated based on the First-principle are shown in **Figure 5**. The calculated band gap is 3.16 eV which is very close to the measured value of 3.11 eV. The valence band maximum (VBM) and conduction band minimum (CBM) are mainly composed of Cu 3d state, and the transition between VBM and CBM is forbidden according to the dipole and spin selection rules. Under the UV radiation, the electrons can be excited from the VB to CB upper level producing the absorption spectra. As measured from the excitation and emission spectra, the large Stoke shift 11 804 cm^{-1} cannot be ascribed to the charge transfer transition from the ligand to Cu 3d state.[36] These two red emissions are originated from Cu(1) $3d^94s^1$–$3d^{10}$ transition and ligand empty π^* orbit to Cu $3d^{10}$ transition of Cu(2).[31] As shown in Figure S2 (Supporting Information), the two Cu sites have different coordination environments. The Cu(1) is coordinated with two S atoms

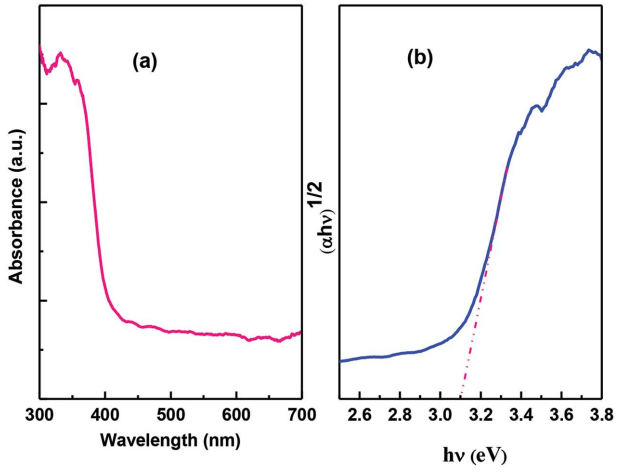

Figure 4. a) Optical absorption spectra and b) the calculated band gap of Cu-Cy.

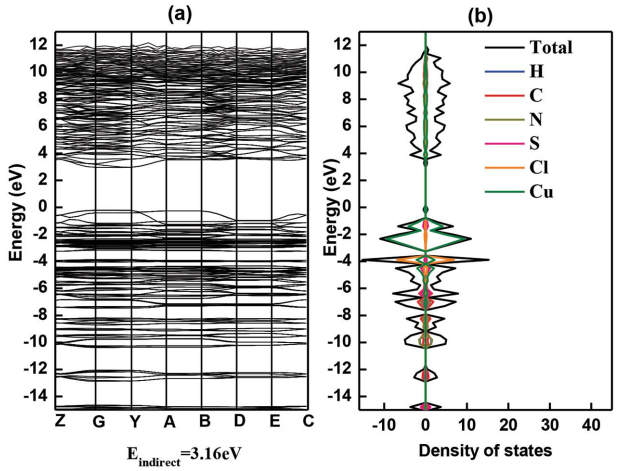

Figure 5. a) Band structure and b) DOS for Cu-Cy calculated by using hybrid DFT.

with a distance of 2.23214 Å and one Cl atom with a distance of 2.29237 Å, while the Cu(2) is coordinated with two S atoms with distances of 2.28301 and 2.32152 Å, respectively, and with one N atom at a distance of 2.08386 Å. For Cu(1) atom, the coordination anion cannot provide empty orbits for electron transitions, thus, the long wavelength (626 nm) emission is corresponding to the $3d^9 4s^1$–$3d^{10}$ transition in Cu(1) site. For Cu(2) site, the coordination N atom forms the sp^3 hybridization with the nonbonding orbits and LP electrons. Therefore, transition between ligand empty π^* orbit and Cu $3d^{10}$ leads to the short wavelength emission at 613 nm.

The emission spectra and CIE (Commission Internationale de L'Eclairage) chromaticity positions of the phosphors with different mass ratios of g-C_3N_4 treated with the 60.7% nitric and Cu-Cy are shown in **Figure 6**. The weight ratio of g-C_3N_4 to Cu-Cy is 1:1.33, 1:1.67, and 1:2.67, respectively. Under 365 nm excitation, the emission extends through the whole visible light region from 400 to 700 nm. The two strong emission peaks at 435 nm (blue) and 616 nm (red) are from the emissions of g-C_3N_4 and Cu-Cy, respectively. The emission spectrum of the composites is a mechanical mixture of their respective emission spectrum, and the luminescent intensity of the component material increases with its ratio in the mixture. **Figure 7**

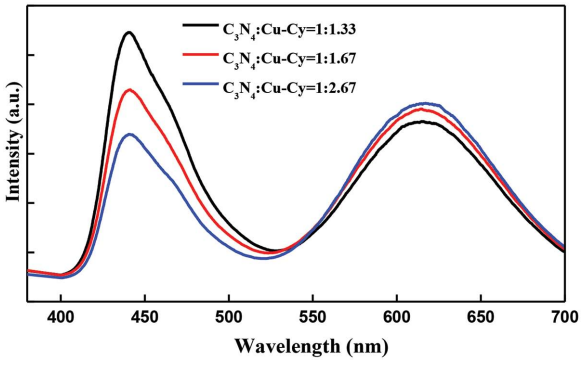

Figure 6. Photoluminescence spectra of phosphors with different weight ratios of the g-C_3N_4 and the Cu-Cy.

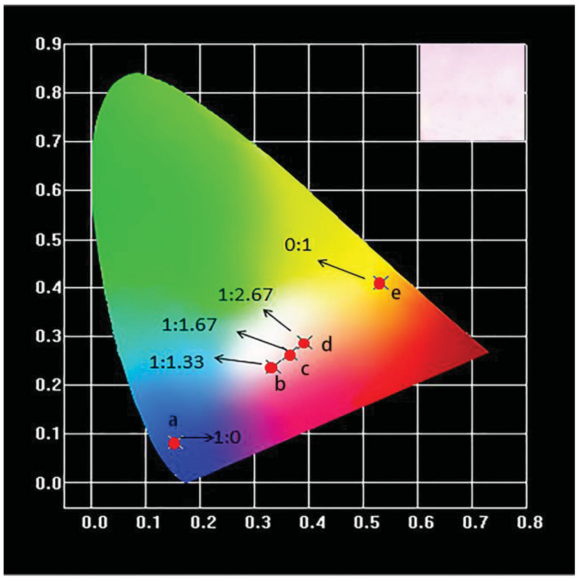

Figure 7. The CIE chromaticity coordinates for phosphors mixed with g-C_3N_4 and Cu-Cy excited at 365 nm and photography of the sample (c) under 365 nm UV lamp excitation.

shows the CIE chromaticity positions of the emission-tunable phosphors excited at 365 nm. The inset is a digital photo of the mixed phosphors (c) excited by a 365 nm UV lamp. As shown in **Table 1**, the color coordinates can be gradually tuned from blue (0.156, 0.083) through white light (0.365, 0.265) toward orange (0.533, 0.409) in the visible spectral region via a systematical changing of the weight ratio of the two materials. When the weight ratio of g-C_3N_4 and Cu-Cy is 1:1.67, the quantum yield (QY) is 20%.

To prove the concept of C_3N_4 and Cu-Cy composites for the white light-emitting diode (WLED) application, a WLED lamp was fabricated by deposition of g-C_3N_4 and Cu-Cy (weight ratio 1:1.67) on a 365 nm near-ultraviolet (NUV) LED chip. The electroluminescence spectrum of the WLED lamp has a broad blue emission at 435 nm from g-C_3N_4 and a broad red emission at 616 nm attributed to Cu-Cy as shown in **Figure 8**. The inset of Figure 8 shows a single-composition WLED lamp and the corresponding white-light emission driven under a forward bias current of 300 mA. The detailed CIE color coordinates, correlated color temperature (CCT), and color rendering index (CRI) of the WLED lamp under forward bias of 300 mA are: $x = 0.352$, $y = 0.320$; 4523 K; and 94.3, respectively.

The spectra of the WLED with different bias currents of the chip are shown in Figure S3 (Supporting Information). It can be

Table 1. The CIE chromaticity coordinates for white light emitting phosphors of g-C_3N_4 and Cu-Cy.

Composition	Mass ratio	CIE *x*	CIE *y*
g-C_3N_4	–	0.156	0.083
g-C_3N_4:Cu-Cy	1:1.33	0.336	0.238
g-C_3N_4:Cu-Cy	1:1.67	0.365	0.265
g-C3N_4:Cu-Cy	1:2.67	0.393	0.287
Cu-Cy	–	0.533	0.409

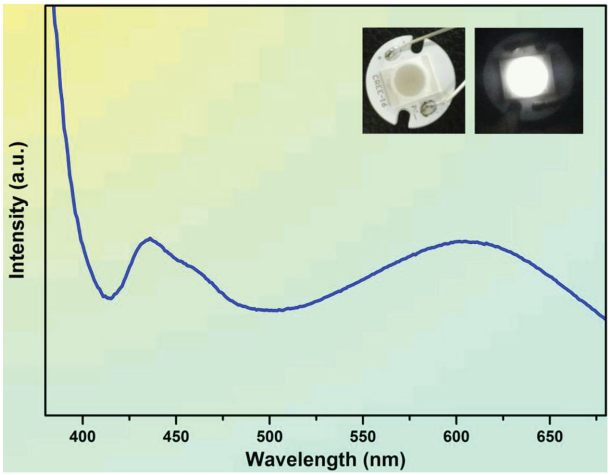

Figure 8. The electroluminescence spectrum of the WLEDs using the phosphor consisting of g-C_3N_4 and Cu-Cy at the forward bias current of 300 mA. Inset: photos of the WLEDs.

seen that the luminescence intensity of the WLED increases when the bias current is from 100 to 150 mA. However, as the bias current is increased to 200 and 300 mA, the emission is decreased.

Figure S4 (Supporting Information) shows the WLED emission spectra at different operating times. Both the blue and the red emissions decrease in intensity with the operating time, and the red emission is decreased faster than the blue one. The peak position of the blue emission is almost the same at different bias currents or operating times, while the red emission peak is shifted to shorter wavelengths. We found that if the lamp was operated at a low current for a short time period, it could recover its luminescence intensity after cooling down. However, after operating at a high current or for a long time period, the luminescence cannot recover after cooling down.

The decrease of the luminescence intensity of the phosphors is mainly due to the increase of the temperature with the bias current or operation times. During the operation, the chip temperature could be higher than 100 °C.[37] Generally, the self-activated luminescence with a large Stokes' shift has a low thermal chromaticity stability, thus the red emission is decreased faster than the blue one.[38,39] Temperature increase is the main reason for the luminescence quenching. In addition, oxidation of the materials is another possible reason. To figure out if the quenching is partially by oxidation, we treated the white-emitting composites at different temperatures in air for 30 min and then measured their luminescence spectra after cooling down to room temperature. As shown in Figure S5 (Supporting Information), the heat treatment of the composites at low temperatures does not obviously influence their luminescence intensity. If the heating temperature is higher than 60 °C, the luminescence intensity decreases but the spectral shape remains almost the same. Also, when the samples are treated at high temperatures in air, we see the samples change color from white to grayish, this means some of the samples were oxidized, and this oxidation is another reason for the quenching of the luminescence which is not recoverable. This issue can be solved by employing the remote-phosphor configuration to reduce the operating temperature of the phosphors.[40,41] In addition, protection and fabrication in vacuum can also help to avoid the quenching and to extend the device lifetime.

It is anticipated that all of the properties of this system can be further improved by optimization such as the LED chip performance, the ratio of epoxy resin to phosphor, and luminescence properties of the phosphors, as well as employing the remote-phosphor LED configuration. It is expected that these materials not only can find applications in solid lighting and displays but also for crop improvement because they can provide the blue emission and the red emission for photosynthesis enhancement.

3. Conclusions

In summary, here, we report new white color composites made of g-C_3N_4 treated with 60.7% nitric acid and Cu-Cy. Under a single wavelength excitaiton at 365 nm, these two materials show strong blue and red luminescence, respectively. The white light emission with a quantum yield of 20% could be obtained by mixing these two self-activated luminescent materials at a weight ratio of 1:1.67. Using a 365 nm NUV chip for excitation, the composites produce a WLED which exhibits an excellent color rendering index of 94.3. These white light materials are environment friendly, easy to approach, and cost-effective. More importantly, this will potentially eliminate the challenge of rare-earth resources. Furthermore, a single chip is used for excitation instead of a multichip, which can greatly reduce the cost of the devices. These materials not only can find applications in solid lighting and displays but also for crop improvement because they can provide blue emission and red emission for photosynthesis enhancement.

4. Experimental Section

Synthesis of the Samples: The g-C_3N_4 powder was obtained through a low temperature thermal condensation of melamine.[27] Briefly, melamine (2 g) was heated at 500 °C in air for 2 h with a heating rate of 3 °C min^{-1} to obtain a yellow powder of g-C_3N_4. g-C_3N_4 yellow powder (1.5 g) was respectively dispersed in nitric acid solutions (25 mL) with concentrations of 34.4, 47.6, and 60.7 wt%, and were heated at 90 °C while stirring for 2 h. Then, the solutions were cooled down to room temperature and the powder samples were precipitated from the solution by centrifugation. Finally, the treated powders were washed several times to remove the acids using deionized (DI) water and then were dried at 70 °C in an air to obtain the white powder samples.

Cu-Cy particles were synthesized according to our method previously reported.[31] Briefly, $CuCl_2{\cdot}2H_2O$ (0.460 g, 2.698 mmol,) was dissolved in DI water followed by addition of cysteamine (0.636 g, 8.244 mmol). After adjusting the pH value to 8 by adding NaOH solution (2.5 mol L^{-1}, 8 mL), the solution was stirred for about 2 h at room temperature and then heated to its boiling temperature for 30 min. Particles of Cu-Cy were obtained by centrifuging and washing the crude product with a solution of deionized (DI) water and ethanol (v/v = 5:4) three times followed by sufficient sonication. Finally, the particles were dried completely in vacuum at room temperature overnight.

Characterization of the Samples: The X-ray diffraction (XRD) was recorded using a Bruker D8-Advance X-ray diffractometer with Cu Ka radiation (λ = 0.15405 nm). The photoluminescence (PL) and photoluminescence excitation (PLE) spectra were measured on an F4500 fluorescence spectrometer. The luminescence quantum yields were measured by an FLS920 spectrofluorometer (Edinburgh Instruments) equipped with integrating sphere. All the measurements were carried out at room temperature. The size and shape of the samples were observed

on a field emission scanning electron microscope (FE-SEM, S-4800 Hitachi) operating at 15 kV and a transmission electron microscope (TEM, JEOL JEM 2100F) operating at 200 kV. The temperature quenching on the luminescent properties of the white-emitting composites was studied by heat treating the composite at different temperatures in the air for 30 min.

Light Emitting Diode (LED) Chip Fabrication: One LED was fabricated by depositing the epoxy resin containing composite made with a ratio 1:1.67 of g-C_3N_4 and Cu-Cy on a 365 nm NUV LED chip. The g-C_3N_4 was treated with nitric acid of 60.7%. The details of the 365 nm NUV chips are as follows: wavelength peak: 365–370 nm; chip size: 45 ± 45 mil^2; forward voltage: 3.5 V; forward electric current: 300 mA. The emission spectra, CRI, CCT, and CIE color coordinates for samples were recorded with a HAAS-2000 system (Yuanfang, China).

Calculation Details: The theoretical calculation was performed using the plane wave and the projector augmented wave (PAW) pseudo-potential method incorporated in the VASP software.[42] The Hybrid density functional theory (DFT) calculation was carried out at a single point with the generalized gradient approximation (GGA) lattice geometry. Firstly, the GGA scheme was employed for the fullyrelaxed structural optimization. Then, the screened-exchange hybrid functional of Heyd, Scuseria, and Ernzerhof (HSE) representing the electronic exchange–correlation energy was adopted during calculation of the DOS and the band structure.[43] The valence configurations including valence and semicore electrons are $1s^2$ for hydrogen, $2s^22p^2$ for carbon, $2s^22p^3$ for nitrogen, $3s^23p^2$ for sulfur, $3s^23p^5$ for chlorine, and $4s^13d^{10}$ for copper according to the PAW scheme.[44] The model structure is based on a 96-atom conventional cell. The cutoff energy was 450 eV and the Monkhorst–Pack K-point mesh for the unit (conventional) cell was $3 \times 1 \times 3$. The structural relaxation of the crystal was carried on until the total energy was converged to 10^{-5} eV and the residual forces on atoms were below 0.02 eV $Å^{-1}$.

Supporting Information

Supporting Information is available from the Wiley Online Library or from the author.

Acknowledgements

This project was financially supported by the National Science Foundation of China (Grant Nos. 91222110 and 51472013), Specialized Research Fund for the Doctoral Program of Higher Education of China (Grant No. 20121102110027), Fundamental Research Funds (Grant No. YWF-15-WLXY-020), State Key Laboratory of New Ceramic and Fine Processing Tsinghua University (Grant No. KF201414), and the high-performance computing platform of Network Information Center in Beihang University.

Received: June 29, 2015
Revised: September 11, 2015
Published online: October 19, 2015

[1] O. Chen, J. Zhao,V. P. Chauhan, J. Cui, C. Wong, D. K. Harris, H. Wei, H. S. Han, D. Fukumura, R. K. Jain, Mo. G. Bawendi, *Nat. Mater.* **2013**, *12*, 445.
[2] C. M. Zhang, J. Lin, *Chem. Soc. Rev.* **2012**, *41*, 7938.
[3] M. Olle, A. Virsile, *Agric. Food Sci.* **2013**, *22*, 223.
[4] L. Wondraczek, M. Batentschuk, M. A. Schmidt, R. Borchardt, S. Scheiner, B. Seemann, P. Schweizer, C. J. Brabec, *Nat. Commun.* **2013**, *4*, 2047.
[5] S. Lian, C. Rong, D. Yin, S. Liu, *J. Phys. Chem. C* **2009**, *113*, 6298.
[6] Q. Xia, M. Batentschuk, A. Osvet, P. Richter, D. P. Häder, J. Schneider, C. J. Brabec, L. Wondraczek, A. Winnacker, *Opt. Exp.* **2013**, *21*, A909.
[7] L. Ma, D. J. Wang, Z. Y. Mao, Q. F. Lu, Z. H. Yuan, *Appl. Phys. Lett.* **2008**, *93*, 144101.
[8] C. S. Brown, A. C. Schuerger, J. C. Sager, *J. Am. Soc. Hortic. Sci.* **1995**, *120*, 808.
[9] S. W. Hogewoning, G. Trouwborst, H. Maljaars, H. Poorter, W. van Ieperen, J. Harbinson, *J. Exp. Bot.* **2010**, *61*, 3107.
[10] L. Sommerdijk, J. M. P. J. Verstegen, A. Bril, *J. Lumin.* **1974**, *8*, 502.
[11] J. Y. Zhang, Z. T. Zhang, Z. L. Tang, Y. Tao, X. Long, *Chem. Mater.* **2002**, *14*, 3005.
[12] W. X. Wang, P. P. Yang, Z. Y. Cheng, Z. Y. Hou, C. X. Li, J. Lin, *ACS Appl. Mater. Interfaces* **2011**, *3*, 3921
[13] J. Llanos, R. Castillo, W. Alvarez, *Mater. Lett.* **2008**, *62*, 3597.
[14] N. Pradal, D. Boyer, G. Chadeyron, S. Therias, A. Chapel, C. V. Santilli, R. Mahiou, *J. Mater. Chem. C* **2014**, *2*, 6301.
[15] J. Wang, X. Jing, C. Yan, J. Lin, F. Liao, *J. Electrochem. Soc.* **2005**, *152*, G534.
[16] M. Groenewolt, M. Antonietti, *Adv. Mater.* **2005**, *17*, 1789.
[17] X. Wang, K. Maeda, A. Thomas, K. Takanabe, G. Xin, J. M. Carlsson, K. Domen, M. Antonietti, *Nat. Mater.* **2009**, *8*, 76.
[18] G. Dong, K. Zhao, L. Zhang, *Chem. Commun.* **2012**, *48*, 6178.
[19] B. Chai, T. Peng, J. Mao, K. Li, L. Zan, *Phys. Chem. Chem. Phys.* **2012**, *14*, 16745.
[20] K. Takanabe, K. Kamata, X. Wang, M. Antonietti, J. Kubota, K. Domen, *Phys. Chem. Chem. Phys.* **2010**, *12*, 13020.
[21] F. Dong, L. Wu, Y. Sun, M. Fu, Z. Wu, S. C. Lee, *J. Mater. Chem.* **2011**, *21*, 15171.
[22] Y. Zhang, J. Liu, G. Wu, W. Chen, *Nanoscale* **2012**, *4*, 5300.
[23] J. Hong, X. Xia, Y. Wang, R. Xu, *J. Mater. Chem.* **2012**, *22*, 15006.
[24] S. C. Yan, Z. S. Li, Z. G. Zou, *Langmuir* **2010**, *26*, 3894.
[25] S. C. Yan, Z. S. Li, Z. G. Zou, *Langmuir* **2009**, *25*, 10397.
[26] Z. X. Ding, X. F. Chen, M. Antonietti, X. C. Wang, *ChemSusChem* **2011**, *4*, 274.
[27] Y. Zhang, Q. Pan, G. Chai, M. Liang, G. Dong, Q. Zhang, J. Qiu, *Sci. Rep.* **2013**, *3*, 1943.
[28] X. D. Zhang, X. X, H. Wang, J. J. Zhang, B. C. Pan, Y. Xie, *J. Am. Chem. Soc.* **2013**, *135*, 18.
[29] X. Zhang, H. Wang, H. Wang, Q. Zhang, J. Xie, Y. Tian, J. Wang, Y. Xie, *Adv. Mater.* **2014**, *26*, 4438.
[30] J. Zhou, Y. Yang, C. Y. Zhang, *Chem. Commun.* **2013**, *49*, 8605.
[31] L. Ma, W. Chen, G. Schatte, W. Wang, A. G. Joly, Y. Huang, R. Sammynaiken, M. Hossu, *J. Mat. Chem. C.* **2014**, *2*, 4239.
[32] L. Ma, X. Zou, W. Chen, *J. Biomed. Nanotechnol.* **2014**, *10*, 1501.
[33] J. Xu, Y. Li, S. Peng, G. Lu, S. Li, *Phys. Chem. Chem. Phys.* **2013**, *15*, 7657.
[34] P. Niu, G. Liu, H. M. Cheng, *J. Phys. Chem. C* **2012**, *116*, 11013.
[35] P Niu, L. L. Zhang, G. Liu, H. M. Cheng, *Adv. Funct. Mater.* **2012**, *22*, 476
[36] A. Vogler, H. Kunkely, *J. Am. Chem. Soc.* **1986**, *108*, 7211.
[37] E. Fred Schubert, J. K. Kim, *Science* **2005**, *308*, 1274.
[38] S. B. Kim, B. G. Kum, H. M. Jang, A. Lakshmanan, B. K. Kang, *J. Lumin.* **2011**, *131*, 1625.
[39] Y. L. Huang, Y. M. Yu, T. Tsuboi, H. J. Seo, *Opt. Express* **2012**, *20*, 4360.
[40] J. K. Kim, H. Luo, E. F. Schubert, J. Cho, C. Sone, Y. Park, *Jpn. J. Appl. Phys.* **2005**, *44*, L649.
[41] S. E. Brinkley, N. Pfaff, K. A. Denault, Z. J. Zhang, H. T. Hintzen, R. Seshadri, S. Nakamura, S. P. DenBaars, *Appl. Phys. Lett.* **2011**, *99*, 241106.
[42] G. Kresse, J. Furthmüller, *Phys. Rev. B* **1996**, *54*, 11169.
[43] J. Heyd, G. E. Scuseria, M. Ernzerhof, *J. Chem. Phys.* **2006**, *124*, 219906.
[44] G. Kresse, D. Joubert, *Phys. Rev. B* **1999**, *59*, 1758.